http://dx.doi.org/10.21611/qirt.1996.022

Heat transfer identification induced by multihole cooling in combustion chambers

by J. Dumoulin[1], M. Marchand[2], P. Reulet[2] and P. Millan[2]

[1]LETHEM / INSA-UPS, Dpt Génie Civil, INSAT, Complexe Scientifique de Rangueil, 31077 TOULOUSE cedex 04, France; [2] CERT-ONERA / DERMES, 2 Av. E. Belin B.P. 4025 - 31055 TOULOUSE cedex, France

Abstract

This paper deals with the identification of the heat transfer occurring in the combustion chambers of turbomachines. Several test plates, reproducing at different scales the walls of combustion chambers have been used to quantify the effectiveness of a 30° staggered multihole cooling. Using a physical model and temperature measurements made by infrared thermography, the behavior of the convection heat transfer coefficient and the adiabatic wall temperature downstream the hole region have been determined. A modification of the model gave their behavior in the perforated area, then correlations of the effectiveness versus the streamwise distance and the blowing ratio were performed.

Nomenclature

D	Hole diameter
Cp	Specific heat
e	Thickness
h	Convective heat transfer coefficient
K	Natural convective heat transfer coefficient

Greek Symbols

λ	Heat conductivity
σ	Stefan constant
ε	Hemispherical emissivity in the 2-5.6 µm band
η	Effectiveness
ρ	Density

Dimensionless Numbers

m	Blowing rate
Bi	Biot number
Nu	Nusselt number

Subscripts

aw	Adiabatic wall
second	coolant
cv	Forced convection
steel	steel
ray	Radiation
conv	Forced convection inside the hole
ext	Surrounding
hot	Hot mainstream

Abbreviations

ThIR	Infrared Thermography

1. Introduction

In order to lighten the aeronautical-vehicle engines and improve their effectiveness, new types of components are used to build the walls of the combustion chambers. Consequently, as they are submitted to increasing thermal loads, cooling schemes are required to raise their lifetime. Among the different types of cooling commonly used we focused on the injection of coolant through multiholes made in the wall of the chamber. Due to the special geometries and conditions of use encountered in such a case, some specific physical models have to be made in order to help the numerical simulations of the phenomenon.
The aerothermic group of the CERT/DERMES has studied this problem for several years [1-3]. A physical modelisation based on the thermal balance of an element of wall [3] coupled with measurements of temperature using Infrared thermography (noted further ThIR) has been achieved. This modelisation, presented below has to be suited to each specific geometry. The present study shows results obtained in the case of a staggered 30° inclined multihole cooling for an injectant to free-stream density ratio near 1.2 and low values of the blowing rate m which represents the coolant to mainstream mass flux ratio.

2. Experimental apparatus

2.1 The wind tunnel

The facility is an open circuit. The flow is generated by two sources of compressed air (figure 1). The first one, a 20 bar compressed air source, gives a maximum of 400 Nm3/h of air which is heated at a maximum temperature of 400°C. It constitutes the hot side of the test section and simulates the flow inside the combustion chamber. The hot test section is a

http://dx.doi.org/10.21611/qirt.1996.022

rectangle of size 68 x 150 mm^2. The cooling flow is given by a 10 bar compressed air source, up to 600 Nm3/h, passing through the holes of the test plate which separates the test section in two parts as represented in Fig. 1. Note that the cold part of the wind tunnel is closed at its end so that the coolant is forced to go through the holes. Since the test section is open, the mixed air downstream the holes is exhausted. Furthermore, several thermocouples measure the temperature of the two streams at different locations in the wind tunnel.

2.2 The test plates

Three models of combustion chambers walls have been studied.
The first one is a 1 mm thick steel plate perforated in its central part. The hole region is made of 1053 staggered holes of diameter 0.5 mm, angled 30° to the surface plate and spaced 3 diameters apart both in the streamwise and spanwise directions. The hole length to diameter ratio is 4.
By its configuration and dimensions, this plate simulates the wall of some combustion chamber with a scaling factor equal to 1.
The second test model is a 9 mm thick steel plate (figure 2) in order to get a scaling factor of 9 with regard to the first plate. The hole diameter is 4.5 mm, the hole length to diameter is preserved. The main difference concerns the number of holes, which for this plate is equal to 7. The purpose is then to zoom in the region of the holes to determine with a good accuracy the thermal loads around the holes. Four thermocouples have been buried at the back of the plate to record the temperature on its cold side.
For complementary measurements, a third test plate with a scaling factor equal to 3 has been used. Its characteristics are: thickness 3 mm, hole length to diameter ratio 4, hole diameter 1.5 mm, number of holes 18.The three plates have been coated with a high emissivity black paint.

2.3 The infrared thermography system

The infrared camera used is a short wave Agema 782 (2 μm-5.6 μm), with a InSb detector cooled by liquid nitrogen. The camera has been calibrated with a black body source available at the DERMES [3]. The spatial resolution of the camera is 5 pixels and its thermal resolution is about 0.1°C at 30°C. The hot side of the plate is viewed through a ZnS window which has been inserted into the wall of the wind tunnel (Fig. 1). This window is transparent to the infrared wavelengths from 2 to 8 μm and can be used at a maximum temperature of 400 °C.

Concerning the first plate, the objective is a 20° lens giving a 150 x 150 mm^2 field of view. This allows to see both inside and downstream the hole region. For the second plate, the objective is a 7 ° lens; the field of view is $45 \times 45 mm^2$ corresponding to a part of the hole region. The thermosignal given by the camera is digitised with the help of a 8 bits A/D converter and stored on a computer.

3. Modelisation

Let us consider a volume element of the plate when this one is subjected to cooling. The energy flux balance on the element can be schemed as :

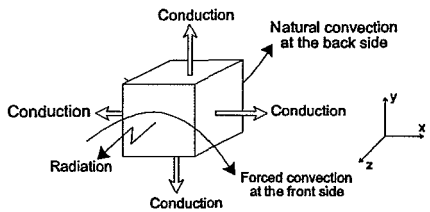

http://dx.doi.org/10.21611/qirt.1996.022

Considering conductive boundary conditions on the lateral faces of the element and the hypothesis that the body is thin ($Bi < 0.1$ **then** $T_{z=0} = T_{z=e}$) we can write [3,4] the system 1 :

System 1:

$$\begin{cases} \text{Equation at time t :} \\ 0 = \rho_{steel} \cdot C_{steel} \cdot e_{steel} \cdot \dfrac{\partial T(x,y,t)}{\partial t} + h(x,y) \cdot (T(x,y,t) - T_{aw}(x,y,t)) + \varepsilon_{steel} \cdot \sigma \cdot (T^4(x,y,t) - T_{ext}^4) \\ \quad - e_{steel} \cdot \lambda_{steel} \cdot \left(\dfrac{\partial^2 T(x,y,t)}{\partial x^2} + \dfrac{\partial^2 T(x,y,t)}{\partial y^2} \right) + K \cdot (T(x,y,t) - T_{second}) \\ \text{Equation at the final time :} \\ 0 = h(x,y) \cdot (T(x,y,t_{final}) - T_{aw}(x,y)) + \varepsilon_{steel} \cdot \sigma (T^4(x,y,t_{final}) - T_{ext}^4) \\ \quad - e_{steel} \cdot \lambda_{steel} \cdot \left(\dfrac{\partial^2 T(x,y,t_{final})}{\partial x^2} + \dfrac{\partial^2 T(x,y,t_{final})}{\partial y^2} \right) + K \cdot (T(x,y,t_{final}) - T_{second}) \end{cases}$$

T(x,y,t) and $T(x,y,t_{final})$ are the front side element temperature for each time t and for the final time, when the thermal equilibrium is reached.

T_{second} is the temperature of the coolant. If we can measure, by ThIR, the values of T(x,y,t) and $T(x,y,t_{final})$, then by solving system 1 we get:

System 2:

$$\begin{cases} h(x,y) = \dfrac{A - B}{T(x,y,t) - T(x,y,t_{final})} \\ T_{aw}(x,y) = \dfrac{\dfrac{A}{B} \cdot T(x,y,t_{final}) - T(x,y,t)}{\dfrac{A}{B} - 1} \\ \text{With :} \\ A = -\rho_{steel} \cdot C_{steel} \cdot e_{steel} \cdot \dfrac{\partial T(x,y,t)}{\partial t} - \varepsilon_{steel} \cdot \sigma \cdot (T^4(x,y,t) - T_{ext}^4) \\ \quad + e_{steel} \cdot \lambda_{steel} \cdot \left(\dfrac{\partial^2 T(x,y,t)}{\partial x^2} + \dfrac{\partial^2 T(x,y,t)}{\partial y^2} \right) - K \cdot (T(x,y,t) - T_{second}) \\ B = -\varepsilon_{steel} \cdot \sigma \cdot (T^4(x,y,t_{final}) - T_{ext}^4) \\ \quad + e_{steel} \cdot \lambda_{steel} \cdot \left(\dfrac{\partial^2 T(x,y,t_{final})}{\partial x^2} + \dfrac{\partial^2 T(x,y,t_{final})}{\partial y^2} \right) - K \cdot (T(x,y,t_{final}) - T_{second}) \end{cases}$$

i.e the instantaneous values of the convective transfer coefficient h and the adiabatic wall temperature Taw.

4. Experimental procedure

Practically, before t=0 the plate is in thermal equilibrium with the hot main stream at a temperature of about 100°C. At t=0, the coolant (20°C) is injected and a temporal thermogramm of the scene (T(x,y,t)) is acquired by the infrared camera. Then, at t_{final} when the thermal equilibrium is reached, a new thermal map ($T(x,y,t_{final})$) is recorded.

The computation is performed, for each 5 pixels large element which represents the resolution of the camera. The discretisation uses a central finite differences scheme.

The instantaneous values of h and Taw are calculated; an average over t gives the map of mean h and Taw for each test plate.

http://dx.doi.org/10.21611/qirt.1996.022

5. Results

5.1 Scale 1 test plate

The experimental procedure has been applied to this plate for different values of the blowing rate (ranging from 2 to 8) leading to maps of h and Taw. By averaging over y (spanwise), one can plot h or Taw versus x, the streamwise distance originating at the end of the hole region. Outside the multihole area, the behavior of h is in good agreement with the literature [5] tending towards the curve of h(x) on a flat plate far from the hole region. Anyway, in the hole region the values of h seem to be overestimated. This can be explained by the fact that the model does not take into account convective boundary conditions on the lateral faces of an element and also, due to the inclination of the holes, the temperature can not be considered independent of z. The scale 9 test plate has then been used and the model has been modified in order to determine the correct values of h and Taw in the hole region.

5.2 Scale 9 test plate

Some detailed measurements have been made on the scale 9 test model for values of the blowing rate ranging from 2 to 22. At the same time, a first approach has been made to take into account the specific conditions in which heat transfer occurs. The original model has been modified on the basis of new hypotheses [6]:

First, for each element, a criterion has been added to know whether a conductive or a convective lateral boundary condition has to be applied. Practically a matrix built with coefficients equal to 1 if the element is made of steel and zero if it is air (inside a hole) is applied to all the elements. For the convective condition, the value of $Hconv$ for each blowing rate has been deduced from the correlations available in the literature [8-10]. It is important to note that the model does not involve more complex boundary conditions such as conduction *and* convection at the same time on one lateral side of the element.

We have also considered that the thickness of the plate which is no more negligible induces a dependence of T versus z. In first approximation we have taken the simplified linear expression, presented below in its discretised form:

$$T(x,y,z,t) = F(x,y,t)z + G(x,y,t)$$

$$with \begin{cases} F(x,y,t) = \dfrac{Tback^{t}_{i,j} - T^{t}_{i,j,e}}{e} \\ G(x,y,t) = T^{t}_{i,j,e} \end{cases}$$

where $T^{t}_{i,j,e}$ is the temperature measured by ThIR for every time at point (i,j) on the hot side and $Tback^{t}_{i,j}$ the temperature at the cold back side of the plate. The latter one has been considered uniform and measured by thermocouples.

Finally, the inclination of the holes has been neglected, each element being considered as a cube. The explicit discretisation of the fluxes for an element submitted on each of its faces to a conductive or a convective flux is given by Lienhard [7]. The new writing of the equations at time t and final time leads to the resolution of the system.
Figure 3 shows a comparison of the values of h on the scale 9 test model for m=5, one calculated with the original model (left) and the other with the modified one (right). This comparison shows that h is twice lower when calculated by the modified model. The same comparison made for the other values of the blowing rate leads to the same results. This has also been confirmed using the intermediate scale plate (scale 3). The adiabatic wall temperature values show the same results.
The error made when calculating h and Taw in the hole region using the original model has then been estimated with accuracy. This has given the complete determination of the transfer on the scale 1 test plate for several values of the blowing rate. Some correlations have been proposed in terms of the spanwise averaged effectiveness:

http://dx.doi.org/10.21611/qirt.1996.022

$$\bar{\eta}=\frac{T_{hot}-T_{aw}}{T_{hot}-T_{second}}$$

versus x/D and m [11].
The correlation $\bar{\eta}(m, x/D)=(0.024m+0.808)\ (x/D)^{(-0.00467m-0.0796)}$ is presented in figure 4 for m=2 and 5.

6. Conclusions and perspectives

By solving physical models with numerical calculations and coupling them to measurements using ThIR, the thermal loads in some specific geometries and conditions of use have been determined. Some correlations have been proposed in order to improve the numerical simulations in such geometries and the perspectives of improving the model are interesting (both conductive *and* convective conditions, inclined elements...).
However, one must be careful when applying the results to the conditions present in the combustion chambers of the turbomachines. Indeed, in the industrial conditions, the blowing rates are higher and the coolant to mainstream density ratios can be 3 or 4 times the tested values.
Higher blowing rates have then to be reached and other dimensionless quantities such as the density ratio between the two fluids have to be looked at. Let us note anyway that for a 30° staggered hole configuration, the influence of the density ratio is known [12], present results could then be directly applied to industrial conditions of use.

7. Acknowledgements

The authors thank M. Plazanet for his technical contribution, the TURBOMECA company and the STPA/TM 94.92003 BC 1 for supporting this work.

REFERENCES

[1] DESCOINS (J.) - *Caractérisation de techniques de refroidissement de paroi: application de le thermographie infrarouge au cas du soufflage parietal.* ENSAE PhD Thesis, Jan.1991.

[2] GIOVANNINI (A.), MILLAN (P.), MEURAT (A.) - *Caractérisation de techniques de refroidissement de paroi: refroidissement par multiperforations (partie 2.).* Technical report n°2398.00/DR/CERT/DERMES, March, 1991.

[3] DUMOULIN (J.) - *Méthodes de détermination, par thermographie infrarouge, des coefficients d'échange de chaleur moyens et instationnaires en aérodynamique perturbée.* INSA PhD Thesis, March, 1994.

[4] DUMOULIN (J.), PLAZANET (M.), RHEULET (Ph.), PLATET (B.) - *Action multiperforations.* Final report n°1/ 2487.00/CI/CERT/DERMES June, 1994.

[5] MARCHAND (M.), DUMOULIN (J.), REULET (Ph.) - *Action multiperforations.* Technical report n°1/ 2538.00 /CERT/DERMES June, 1995.

[6] TAINE (J.), PETIT (J.P.) - *Cours de Transferts thermiques- Mécanique des fluides anisothermes.* Handbook, 1989, Dunod University.

[7] LIENHARD (J. H.) - A heat transfer textbook. Second Edition, 1987, Prentice Hall, INC.

[8] MAC ADAMS (W.H.) - Heat transmission. Handbook, 3rd edition, 1954, p 225.

[9] LATZKO (H.) - Maths U. Mech. NACA TM 1068, 1944.

[10] MILLS (A. F.) - *Experimental investigation of turbulent heat transfer in thermal entrance region of a circular conduit.* J. Mech. Eng. Sci., vol 4, n°1, 1962.

[11] MARCHAND (M.), DUMOULIN (J.), REULET (Ph.) - *Action multiperforations.* Technical report N°2/ 2538.00 /CERT/DERMES Oct.,1995.

[12] AMMARI (H. D.), HAY (N.), LAMPARD (D.) - Journal of turbomachinery. vol.112, July, 1990.

http://dx.doi.org/10.21611/qirt.1996.022

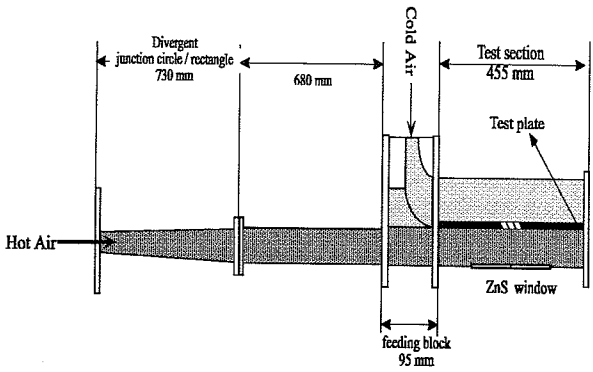

Fig 1:Test section including the test plate

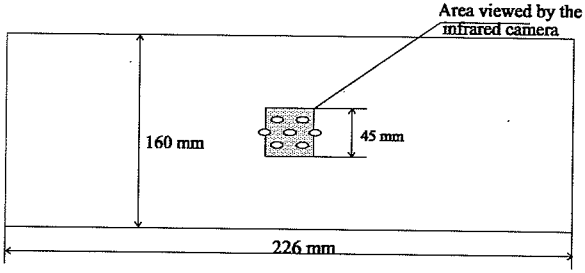

Fig 2: Scale 9 test plate

Fig 3: *See colour figures section*

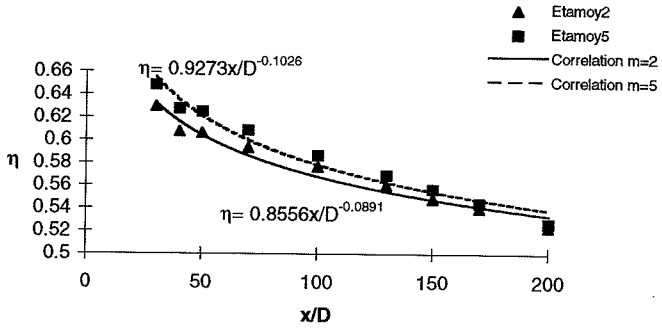

Fig 4: Correlation of η versus x/D for blowing ratios 2 and 5.